Combustion Response Function Measurements by the Rotating Valve Method

R. S. BROWN,* J. E. ERICKSON,† AND W. R. BABCOCK‡
United Technology Center, Sunnyvale, Calif.

A study has been conducted to evaluate the rotating valve method of measuring the combustion response of solid propellants to small amplitude pressure oscillations. The method is based on producing pressure oscillations in a small rocket motor by varying the area of a secondary exhaust nozzle in a periodic manner. This is accomplished by using a rotating valve as the secondary orifice. The valve apparatus operates concurrently with a primary nozzle which controls the steady-state pressure. The frequency of the oscillations is determined by the rotational speed of the valve. A theoretical analysis was conducted to relate the combustion response function to measurable ballistic properties of the combustion chamber. Assuming that the combustion chamber is small in comparison to the acoustic wavelength, the combustion response function can be calculated from the amplitude of the oscillating pressure and the phase angle between the oscillating pressure and oscillating nozzle area. Cold flow tests were conducted using nitrogen and helium to test the validity of the analysis. Excellent agreement was found between the measured and predicted amplitudes and phase angles. Combustion tests then were conducted using two aluminized propellant formulations and three nonaluminized formulations. There was excellent agreement between the T-burner and rotating valve tests conducted on the same batch of propellant. For two non-aluminized propellants, the comparisons were based on different batches of propellant. Differences in combustion response and variations in burning rate and characteristic exhaust velocity were observed for these two formulations. It was concluded that the rotating valve method is a valid substitute for the T-burner. Substantial reductions in the cost of characterizing propellants also were obtained using this new approach.

Nomenclature

A_1 = dynamic combustion parameter
A_b = burning area of propellant grain
A_b^r = real part of acoustic admittance of the combustion
a_n = Fourier cosine coefficient for nth harmonic
A_n = nozzle acoustic admittance
A_t = total area of exhaust ports
b_n = Fourier sine coefficient for nth harmonic
c^* = characteristic exhaust velocity
C_p = specific heat at constant pressure
C_v = specific heat at constant volume
f = frequency
f_a = acoustic frequency
g_c = gravity constant
Im = imaginary part
$\bar{M}_b$ = Mach number of gases leaving the combustion zone
n = burning rate pressure exponent
P = chamber pressure
Q_1 = dynamic combustion parameter
$\dot{r}$ = propellant linear burning rate
R = gas constant
R_1 = dynamic combustion parameter
Re = real part
t = time
T = temperature of the combustion gases
T_f = propellant flame temperature
T_r = $(4\alpha_t g_c A_{t0} R T_f)/(V_c c_0{}^* \dot{r}_0{}^2)$
V_c = volume of combustion cavity
α = growth constant
α_d = decay time constant
α_g = growth time constant
α_t = thermal diffusivity of the solid propellant
γ = C_p/C_v
ε = $\tilde{P}/P_0$, the dimensionless pressure amplitude
θ = phase angle between pressure and area oscillations
λ = $8\pi f \alpha_t/\dot{r}_0{}^2$
λ_1 = defined by Eq. (9)
μ = $\tilde{r}/\dot{r}_0$, the dimensionless burning rate amplitude
ρ = density of combustion gases
ρ_p = propellant density
τ = $\dot{r}_0{}^2 t/4\alpha$
ψ = $\tilde{A}_t/A_{t0}$, the dimensionless area amplitude
ω_f = $\tilde{T}_f/T_{f0}$, the dimensionless flame temperature amplitude
ω = $\tilde{T}/T_0$, the dimensionless temperature amplitude

Superscript
$'$ = instantaneous quantity
$\sim$ = complex amplitude

Subscript
am = amplitude
0 = steady-state value

Presented as Paper 72-1054 at the AIAA/SAE 8th Joint Propulsion Specialist Conference, New Orleans, La., November 29–December 1, 1972; received October 16, 1973; revision received May 14, 1974. This work was supported by the Air Force Rocket Propulsion Laboratory under Contract F04611-72-C-0007. R. J. Schoner and L. E. Stamets were the project engineers. The authors wish to thank R. J. Muzzy for his contributions to the formulation of the study and P. G. Willoughby for his design of an early version of the rotating valve.

Index category: Combustion Stability, Ignition, and Detonation.

* Chief Combustion Research Section. Member AIAA.
† Research Engineer.
‡ Senior Staff Scientist.

Introduction

THE stability of the combustion pressure in a solid propellant rocket motor is determined by a delicate balance between the sources and losses of oscillatory energy. The primary sources of oscillatory energy are the flowfields in the combustion chamber (mean flow driving) and the dynamic combustion properties of the propellant (combustion response). Among the losses are the dynamic flow properties of the nozzle (nozzle damping), the drag losses of the particulate combustion products (particle damping), and the vibration characteristics of the propellant grain and motor case (structural damping). Each of these processes must be characterized quantitatively to predict the over-all stability of a specific propellant in a specific motor.

The dynamic combustion properties of propellants have received particular attention because they constitute a large

energy source and because they are the most difficult to characterize analytically. Several studies[1-4] have been conducted to develop methods for predicting the dynamic combustion response. Each of the resulting theoretical expressions contains a number of chemical and physical parameters which are difficult to determine independently. Thus, for the propellant formulator and the motor designer, these theoretical expressions have little value. Consequently, experimental methods have been sought to obtain the data required for predicting the stability of proposed motor designs.

The T-burner has been the primary experimental method for measuring the combustion response. In this apparatus, propellant is placed in both ends of a tube while the vent is located at the midpoint. The length of the tube determines the frequency of the pressure oscillations, and the combustion pressure is determined by prepressurizing with an inert gas. The primary measurement is the time constant α of the exponential rate of change of the oscillating pressure amplitude with respect to time.

For aluminized propellants, the T-burner can be operated in three modes. In the variable-area mode, the pressure oscillations grow spontaneously and the combustion characteristic (i.e., the combustion response function) is determined by measuring the increase in the growth time constant with increases in the burning surface area. In the pulse mode, the burning area is small and the oscillations do not occur spontaneously. Rather, a small charge is fired during combustion to generate a small pressure disturbance, the amplitude of which decays exponentially with time. A second charge is fired immediately after burnout and the difference between the two measured exponential decay time constants is used to derive the combustion response function. The third mode is a combination of the first two methods. Small charges are fired during the combustion, as in the pulse mode; however, exponential time constants of the pulse decay are measured as a function of burning surface area. The combustion response is determined from the slope obtained from a plot of exponential time constant vs the burning surface area, as in the variable-area method.

Several studies[5-11] have been conducted to evaluate these various methods of operating the T-burner. While the results have been encouraging, it is apparent that there are shortcomings with the T-burner. Fifteen to twenty tests must be conducted to obtain a value of the combustion response at one specific frequency and pressure. In motor development programs in which there are often several candidate formulations to be evaluated, a range of frequencies to be considered, and several pressures to be considered, the T-burner is an expensive method for screening candidate propellants.

In addition, there are theoretical uncertainties[12,13] in the equations used to derive the combustion response function from the T-burner data. These are associated with vent losses and flow losses resulting from turning acoustic flows. The ultimate effect is to produce a $\pm 30\%$–$\pm 50\%$ uncertainty in the combustion response function. These uncertainties also carry over to the stability evaluation of a proposed motor design. Since the stability is determined by relatively small differences in large numbers, a large uncertainty in one of the individual contributions can significantly affect the stability prediction of a motor.

In view of these shortcomings, consideration was given to the development of alternative methods for characterizing the combustion response of solid propellants. This report presents the results of a program conducted under AFRPL Contract F04611-72-C-0007 to explore the rotating valve method for measuring the combustion response function.

Description of the Rotating Valve Method

In the rotating valve method, a small rocket motor is test fired using a conventional nozzle to control the combustion pressure. In addition, a secondary exhaust orifice is periodically opened and closed by a specially designed rotating valve to generate small amplitude pressure oscillations in the rocket motor. The frequency of the oscillations is controlled by the rotational speed of the rotating valve. Thus, small amplitude pressure oscillations are generated in the motor at a selectable pressure and frequency. The amplitude and phase of these pressure oscillations relative to the exhaust area oscillations depend on the transient combustion properties of the propellant and the dynamic ballistic of the chamber.

Theoretical Analysis

To develop the amplitude and phase relationships quantitatively, consider a rocket motor which is short in comparison to the acoustic wavelength. The pressure oscillations are thereby distributed rapidly throughout the chamber and the resulting oscillating pressure is spatially uniform. Under these conditions,[14-17] the mass balance for the chamber is

$$\frac{d(\rho V_c)}{dt} = \rho_p \dot{r} A_b - g_c P A_t / c^* \tag{1}$$

while the energy balance is

$$\frac{d(\rho C_v V_c T)}{dt} = \rho_p \dot{r} A_b C_p T_f - g_c P A_t C_p T / c^* \tag{2}$$

Equations (1) and (2) can be normalized by dividing by the time average mass and energy flow through the combustion chamber. The resulting normalized equations then can be linearized by using the following relations:

$$\dot{r}/\dot{r}_0 = 1 + (\mu/\varepsilon)\varepsilon \exp(i\lambda\tau) \tag{3a}$$

$$P/P_0 = 1 + \varepsilon \exp(i\lambda\tau) \tag{3b}$$

$$A_t/A_{t0} = 1 + \psi \exp(i\lambda\tau) \tag{3c}$$

$$T/T_0 = 1 + \omega \exp(i\lambda\tau) \tag{3d}$$

$$T_f/T_{f0} = 1 + \omega_f \exp(i\lambda T) \tag{3e}$$

$$c^*/c_0^* = 1 + \frac{\omega}{2} \exp(i\lambda\tau) \tag{3f}$$

In Eq. (3a), the complex combustion response function (μ/ε) characterizes the amplitude and phase relationship between the burning rate oscillation and the pressure oscillation.

Substituting Eqs. (3a–3f) into the normalized form of Eqs. (1) and (2) yield

$$\frac{\psi}{\varepsilon} = \left(\frac{\mu}{\varepsilon}\right) + \left(\frac{\omega_f}{\varepsilon}\right)\left\{\frac{0.5 + i\lambda/T_r}{1 + i\lambda/T_r}\right\} - \left\{1 + \frac{i\lambda}{\gamma T_r} + \left(\frac{\gamma - 1}{2\gamma}\right)\frac{i\lambda/T_r}{1 + i\lambda/T_r}\right\} \tag{4}$$

The details of this derivation are presented in the appendix.

For small motors and frequencies above 200 Hz, $\lambda/T_r \gg 1$ and Eq. (4) reduces to

$$Re\left\{\left(\frac{\mu}{\varepsilon}\right) + \left(\frac{\omega_f}{\varepsilon}\right)\right\} = 1 + (\gamma - 1)/2\gamma + \frac{\cos\theta}{(\varepsilon/\psi)_{am}} \tag{5}$$

$$Im\left\{\left(\frac{\mu}{\varepsilon}\right) + \left(\frac{\omega_f}{\varepsilon}\right)\right\} = \frac{\lambda}{\gamma T_r} + \frac{\sin\theta}{(\varepsilon/\psi)_{am}} \tag{6}$$

Thus, given the frequency and ballistic properties of the motor, Eqs. (5) and (6) permit calculation of the combustion response from measured values of the phase angle and the pressure amplitude.

This analytical approach is similar to the one developed concurrently and independently by Barrère and Nadaud.[17] The principal difference between Barrère's results and Eqs. (5) and (6) is that Barrère neglected the energy equation. There is good theoretical[3] and experimental[18] evidence which suggests that this assumption is not valid. Furthermore, Culick[12] has shown that temperature effects are important in T-burner and motor stability analyses. To compare this method wth the T-burner, it is important to know how the temperature effects influence the data analysis.

The effect of flame temperature oscillations also is important when the rotating valve results are used in motor stability predictions. Culick[12] and Cantrell and Hart[19] have shown that the primary combustion driving of acoustic oscillations in a

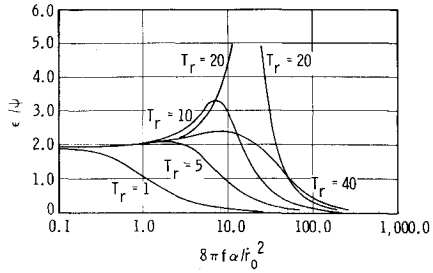

Fig. 1 Predicted amplitude for UTX-8501 propellant ($\gamma = 1.18$).

rocket motor is given by the parameter $(A_b{}^r + \bar{M}_b)$. By a simple mass balance, it can be shown that

$$A_b{}^r + \bar{M}_b = \gamma \bar{M}_b \, Re\,[(\mu/e) + (\omega_f/\varepsilon) - (\gamma - 1)/\gamma] \tag{7}$$

Thus, the phase and amplitude measurements can be related through Eqs. (5) and (7) to the parameter required in motor stability evaluations.

Feasibility Studies

Equations (5) and (6) also can be used to estimate the performance of the proposed experimental system, provided some estimate for the combustion response function can be made. Data for metallized propellants are limited; however, data for nonmetallized propellants are available and can be used for estimating system performance. It should be emphasized that these estimates can be completely misleading, since the effect of metal combustion on the response function of the propellant is unknown.

For nonmetallized propellants Culick[3] and Brown and Muzzy[4] have shown experimentally and theoretically that the combustion response function can be correlated with reasonable accuracy

$$\left(\frac{\mu}{\varepsilon}\right) = Re\left(\frac{\mu}{\varepsilon}\right) + i\,Im\left(\frac{\mu}{\varepsilon}\right) = \frac{n(1 + A_1 - R_1) + Q_1(\lambda_1 - 1)}{\lambda_1 + A_1/\lambda_1 - R_1} \tag{8}$$

where

$$\lambda_1(\lambda_1 - 1) = i\lambda/4 \tag{9}$$

The parameters A_1, R_1, Q_1, and n account for the various propellant chemical and physical properties. As noted earlier, while these parameters have theoretical significance, they cannot be calculated from combustion theory. However, T-burner results have been correlated with Eq. (8) to determine appropriate values for these parameters for nonaluminized propellants.

One set of these parameters from Ref. 4 has been used to estimate the expected amplitude and phase response. The results are shown in Figs. 1 and 2. In these calculations, γ of 1.18 was assumed. In this analysis, the amplitude-frequency behavior (Fig. 1) is similar to the response of a spring-mass-dash pot system when driven by a sinusoidal forcing function. The parameter (T_r) is the ballistic time constant ratio and is somewhat analogous to the damping ratio. However, the phase behavior (Fig. 2) does not follow the analogy to the mechanical system because of the combustion phase lag relative to the pressure. In Fig. 2, the pressure lags the area oscillation by 180° at very low frequencies (i.e., $\lambda < 1$). This reflects the fact that the pressure increases as the nozzle area decreases. For $\lambda > 1.0$, the phase angle depends on the value of T_r. For $T_r < 10$, the phase lag increases with increasing frequency and eventually reaches a limiting phase lag of 270°. However, for $T_r > 10$, the phase decreases with increasing frequency and reaches a limit of a 90° phase lead. The difference between these two types of behavior depends on the magnitude of $\mathrm{Im}(\mu/\varepsilon)$ relative to $\lambda/\gamma T_r$ in the region $1.0 < \lambda > 10$.

Determining the appropriate operating region for the rotating valve (Figs. 1 and 2) requires consideration of a number of factors. First is a consideration of the linear combustion operation of the system. Theoretical calculations[4] suggest that pressure oscillations which are 10% of the steady-state pressure are an upper limit. At levels less than 10%, the combustion response function is a linear property of the combustion and, therefore, does reflect the response of the propellant to small pressure oscillations. Second, small motors and, hence, small steady-state nozzle diameters are necessary to minimize costs. To prevent valve fouling, valve throat diameters must have dimensions similar to the steady-state nozzle diameter. These factors limit the useful region to low values of the amplitude ratio ($\varepsilon/\psi < 0.2$).

The third consideration is the frequency range at which these amplitudes occur. For a propellant with an $\dot{r}_0$ of 0.4 in./sec at 500 psi and an $\alpha = 3.0 \times 10^{-4}$ in.^{2}/sec, a frequency of 1000 Hz is equivalent to a λ of 45. Since typical micromotors have characteristic lengths of 50–75 in. for this burning rate range, the T_r for this propellant-motor combination would be 4. For this λ and T_r, an amplitude ratio of 0.10 would be expected. If

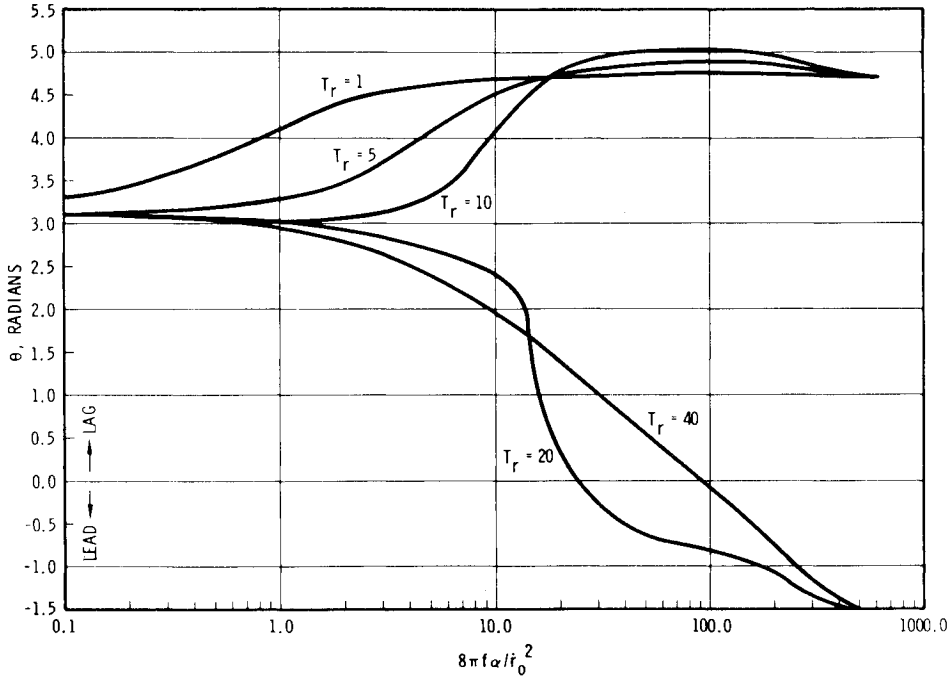

Fig. 2 Predicted phase angle for UTX-8501 propellant ($\gamma = 1.18$).

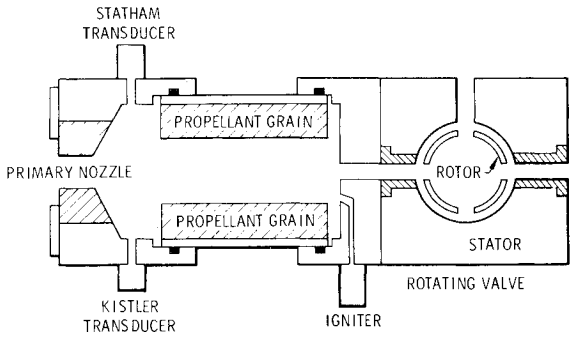

Fig. 3 Apparatus schematic.

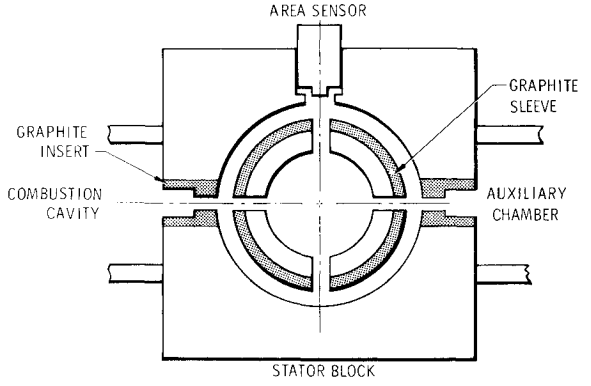

Fig. 5 Rotating valve schematic.

$\psi_0 = 0.5$, the pressure amplitude would be 25 psi peak to peak, which is easily measured with a Kistler transducer and is well within linear system requirements. The phase angle would be 4.8–4.9 rad which also can be measured by careful experimentation. From these calculations, it appears the rotating valve concept can produce signals which can be readily measured in the frequency and pressure amplitude range of interest.

Description of Experimental Apparatus

To evaluate the approach experimentally, a rotating valve was constructed and attached to a small rocket motor. The essential features of this apparatus are shown in Figs. 3 and 4. The valve was connected to the head end of the motor case by a short passage. The primary flow passage was made of replaceable graphite to minimize erosion of metal components. A gaseous oxygen/methane ignition system was located on the side of the motor. A distributor passage was provided inside the motor so the igniter combustion products were directed over the entire propellant surface. This system was extremely reliable and provided rapid ignition of the entire grain surface.

The motor case had an internal diameter of 1.5 in. and a length of 2.75 in. The propellant grains had an initial port diameter of 1.0 in. and were not inhibited on the ends. This design provided an essentially neutral burning grain so that propellant burning rate and c^* data could be obtained concurrently with the dynamic combustion response data.

Pressures were measured by transducers in the aft closure. The steady-state chamber pressure was detected by a Statham model 3532 strain gage transducer, and the oscillating component was measured by a Kistler model 601A1 transducer. The ports to the Kistler were filled with silicone oil prior to each test to eliminate acoustic pressure effects in the transducer line.

The novel component of the equipment was the rotating valve which is shown in Figs. 5 and 6. The rotor was equipped with a replaceable graphite sleeve around the outside circumference. A series of 20 holes 0.156 in. in diameter was drilled in the graphite sleeve on 0.312-in. centers. These holes are aligned with the port in the stator, so that as the rotor was turned the combustion chamber was periodically vented.

Considerable attention was given to the shape of the area wave produced by the valve. As indicated earlier, accurate phase angle measurements are required. Hence, phase errors produced by harmonic components in the area wave were minimized by tailoring the geometry of the graphite insert in the stator. Two possible geometries were considered in detail: 1) a slot with a width identical to the hole diameter in the rotor sleeve, and 2) a circular hole of identical diameter. A Fourier analysis of the wave produced by both geometries is shown in Table 1.

Table 1 Harmonic analysis

Harmonic wave n	Hole/slot a_n	Hole/slot b_n	Hole/hole a_n	Hole/hole b_n
0	0.5	0.0	0.4247	0.0
1	−0.4595	0.0	−0.4252	0.0
2	0.0	0.0	0.0420	0.0
3	−0.0255	0.0	−0.0375	0.0
4	0.0	0.0	0.0122	0.0
5	−0.0069	0.0	−0.0126	0.0
6	0.0	0.0	0.0058	0.0

From these results, it is apparent that the slot is preferred for several reasons. First, the first harmonic content is higher, 91.9% vs 85.0%. Second, the slot eliminates the even harmonics. This makes it substantially easier to filter electronically the oscillating pressure and area signals to reduce the harmonic content still further. It should also be noted that the value of

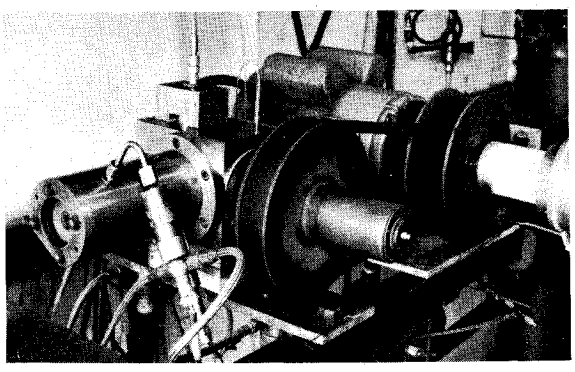

Fig. 4 Experimental apparatus.

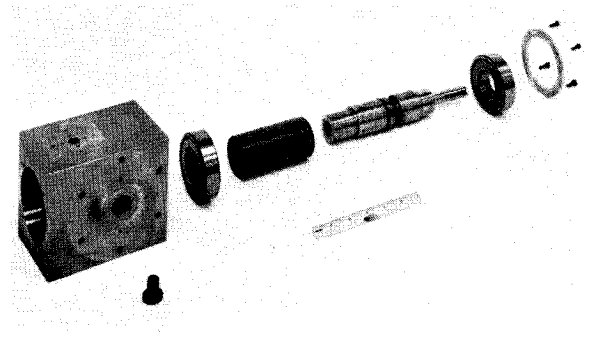

Fig. 6 Rotating valve.

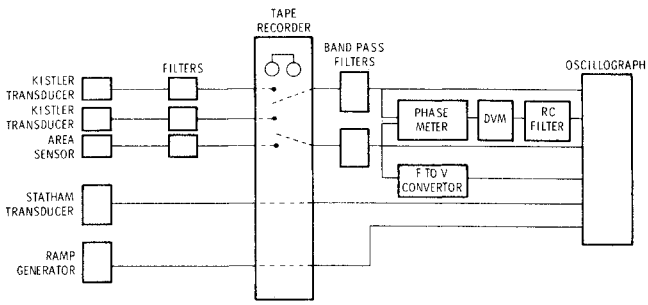

Fig. 7 Electronic data processing equipment.

$a_0 = 0.5$ indicates that the wave is symmetric. This determines the fraction of the vent area to be added to the primary nozzle area to yield the time average total nozzle area.

The instantaneous valve area was measured by machining a second passage in the stator (Fig. 5). This second passage was located precisely 90° (±0.0005 in.) to the first port, but was displaced along the axis of rotation. A second series of ports also was machined in the rotor sleeve to correspond (±0.0005 in.) in rotational position to the first series of rotor ports. However, they were displaced in axial position to correspond to the second passage in the stator. Thus, as the valve turned, there were two passages: one for venting the chamber and one for measuring the instantaneous position of the valve. These very tight dimensional tolerances were critical to the phase measurement. A 0.001-in. displacement from the centerline of either of the ports meant a phase angle error of 0.02 rad.

Two methods for measuring the instantaneous position of these secondary ports were used. The first was based on an electrostatically charged probe. A brass disk was covered with Teflon and inserted precisely into the second passage in the stator. The Teflon was charged electrostatically by rubbing with tissue. The brass then was connected to an extremely high input impedence amplifier (a Kistler model 504D charge amplifier). The ground side was connected to the stator, thereby causing the gap between the brass disk and the rotor to become the dielectric medium of a charged capacitor. As the rotor turned, the dielectric constant between the two electrodes varied as the rotor ports passed close to the Teflon-coated brass disk. This produced an oscillating voltage which is directly related to the vent area.

The center of the charged Teflon-covered disk was located precisely (±0.0005 in.) on the centerline of the stator passage. Several probe designs were tested, but the best results were obtained using a 10° conical surface with the point on the centerline. A thin Teflon sheet stretched over the conical surface was superior to a sprayed coating for two reasons. First, the coating process required curing the Teflon at 750°F for several hours which destroyed the dimensional tolerances of the brass disk. Second, the Teflon had to be replaced frequently and the stretched sheet met this need very well.

The primary advantage of the probe was that it provided a direct measure of the instantaneous valve area. This approach operated very satisfactorily during the cold flow calibration tests, but difficulties were experienced during the combustion tests. The charge on the Teflon was subject to partial neutralization by moisture leaking past the O-ring seal. Thus, contamination of part of the probe surface caused displacement of the center of the electrostatic charge, thereby producing an error in the measured phase angle.

A simple, though indirect, alternative method for measuring the phase angle was developed. It was noted that the cold flow results followed the behavior predicted in Eqs. (5) and (6). An auxiliary cold flow chamber was constructed to operate simultaneously with the combustion chamber. A third port was machined in the stator. This port was located at the same axial position but directly opposite the vent from the combustion chamber (Fig. 5). A small (1.4 in.^{3}), short (1.75 in.) ballistic chamber was attached to the stator and inert nitrogen or helium was injected into this chamber through a sonic choke. This gas was exhausted from this chamber through a slotted graphite insert identical to the one in the main combustion chamber.

As in the main combustion chamber, the chamber pressure was controlled by a steady-state exhaust nozzle, and pressure oscillations were generated by the slot and the rotating valve. The oscillating pressure was monitored with a Kistler model 601A1 pressure transducer and the mean pressure by a Statham strain gage transducer. Assuming the ballistic equations apply with $(\mu/\varepsilon) = \omega_f/\varepsilon) = 0$ for the cold flow tests, the phase relationship between the valve area and the oscillating pressure in the ballistic chamber is known. Hence, by measuring the phase relation between the oscillating pressures in the ballistic chamber and the combustion chamber pressure and by correcting for the ballistic chamber effect, the phase between the combustion chamber pressure and the area can be determined.

A schematic diagram of the electronic data processing equipment is shown in Fig. 7. The signals from the two Kistler transducers, area sensor, and steady-state transducer were recorded on an FM equipped magnetic tape recording system. A ramp generator also was used to indicate the elapsed time during the test. Thus, at large time expansions the data could be sampled to examine several cycles and the elapsed time of that data sample could be determined.

In this apparatus, the Kistler transducer must be operated at high sensitivities to detect the small oscillating pressure. Concurrently, a relatively large signal resulting from the ignition transient also is detected by the Kistler system. This latter part of the signal must be eliminated to prevent saturation of the tape system. The obvious approach is to filter the oscillating pressure signal with a high pass filter. However, considerable care must be taken to eliminate phase angle errors. Both the oscillating pressure and area signals have some harmonic content which can be distorted by filtering. Further, the harmonic content of the two pressure signals probably differs considerably from the harmonic content of the static charge probe signal. Passive electronic filters cannot be used to eliminate the ignition transient since the phase shift is frequency-dependent. Therefore, an active filtering circuit was developed to provide constant gain and zero phase shift for frequencies between 200 and 5000 Hz.

On playback, the oscillating signals were filtered using a variable band-pass filter which attenuated the second harmonic amplitude 20 db. The third harmonic is down 25 db relative to the fundamental (Table 1). After filtering, it is further attenuated to be at least 45 db from the fundamental. This results in a maximum error due to harmonic distortion in the phase angle measurement of 0.005 rad. The filtered signals then were recorded on a CEC model 124 oscillograph. The phase angle was determined electronically using a WAVETEK model 740 phase meter. The phase meter output was fed to a Keathley model 160 Digital Multimeter and then through a simple RC low-pass filter to the oscillograph. A frequency-to-voltage converter was used to determine the frequency electronically and to record the value on the oscillograph record.

A typical test was replayed three times: first to measure the phase relation between the auxiliary chamber oscillating pressure and the area sensor, second to measure the phase relation of the main combustion chamber oscillating pressure and the area sensor, and third to measure the phase between the two oscillating pressures.

Considerable care was taken to insure that the channels used to record the oscillatng signals did not contain phase errors. End-to-end testing using an oscillator showed the phase shift to be less than 0.005 rad. The biggest source of error is the tuning of the variable band-pass filters. Prior to the playback of each test, these two filters were tuned to the desired frequency. The relative phase of the filter outputs also was examined to insure the error was less than 0.005 rad. Thus, the data gathering and processing system provides phase angle measurements to ±0.015 rad. At an amplitude ratio of 0.03, the resulting error in the response function is ±0.5.

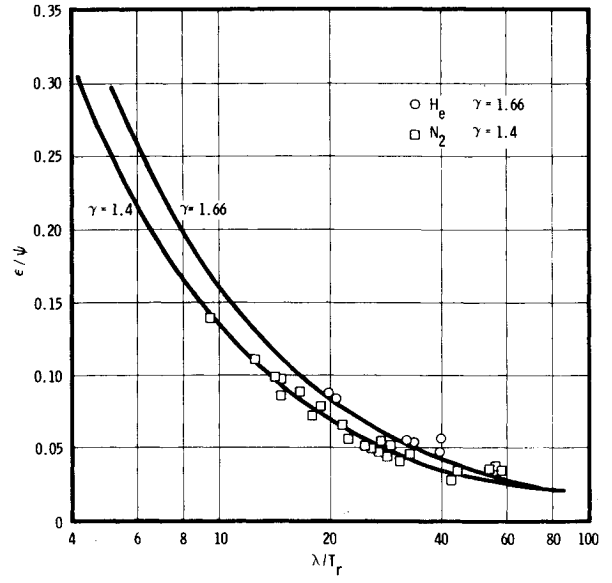

Fig. 8 Cold flow amplitude response of the combustion chamber.

Experimental Results

Cold Flow Tests

Cold flow tests were conducted to evaluate the performance of the motor cavity under conditions where the properties of the gas source could be defined quantitatively. This was accomplished by injecting high pressure nitrogen into the motor cavity through the head end of the igniter. A sonic choke, for which the response function is zero, was used to control the gas flow. Additional tests were conducted with helium to simulate the sonic velocity of the combustion gases. The steady-state nozzle was sized to yield an average chamber pressure of 120 psi and produced an area amplitude of 21%. The static charge probe was used to measure the instantaneous area. Both empty motor cases and simulated propellant grains were used to examine the effect of chamber volume. The tests were conducted over a frequency range of 100–400 Hz using nitrogen and 350–900 Hz using helium.

The experimental amplitude and phase angle data obtained using both helium ($\gamma = 1.66$) and nitrogen ($\gamma = 1.4$) are compared in Figs. 8 and 9 with values predicted from Eqs. (5) and (6). These comparisons show that the ballistic equations characterize the chamber dynamics for λ/T_r (dimensionless frequency) values below 40–45 for nitrogen. This corresponds to an upper frequency limit of 400 Hz, which is approximately 0.35 times the fundamental acoustic frequency of the chamber. The results obtained using helium also are shown in Figs. 8 and 9. From the limited number of tests with this gas, the upper frequency limit is about 850 Hz ($\lambda/T_r = 33$) or approximately 0.26 times the acoustic frequency. Thus, the deviations from the predicted behavior appear to be related to the acoustical frequency of the cavity. They become significant when the test frequency approaches 0.25–0.3 times the acoustic frequency of the chamber.

The studies of Culick and Dehority[20] provide an approximate estimate of the frequency at which momentum (acoustical) effects become important. For nozzles with oscillating throat area, the admittance of the nozzle is

$$A_n = \gamma \bar{M} \left\{ \left(\frac{\gamma - 1}{\gamma} \right) + \frac{\psi}{\varepsilon} [\cos\theta - i \sin\theta] \right\} \tag{10}$$

At the cold flow test frequencies, the imaginary part of the admittance is large compared to the real part since $\theta \cong 3\pi/2$. Culick and Dehority show that under these conditions the pressure amplitude follows the predictions of Eqs. (5) and (6) until $f/f_a \cong 0.25$. For higher frequencies, the amplitude will begin to increase with increasing frequency. This point of departure corresponds to the frequency ratio where amplitude deviations were observed experimentally.

The analysis also predicts phase angle deviations would be expected when $f/f_a \geqq 0.25$. Furthermore, the deviations would produce measured phase angles which are larger than the predicted values. This corresponds to the experimentally observed results. Thus, it was concluded that the observed deviations result from momentum effects. However, for $f/f_a < 0.25$, these cold flow results indicate that Eqs. (5) and (6) can be used to characterize the chamber ballistics and, hence, can be used to derive the combustion response function from combustion tests. For most propellants, this limits the upper frequency to approximately 800 Hz in the apparatus used in this study.

Concurrent with the cold flow tests of the combustion chamber, cold flow tests of the auxiliary chamber also were conducted. These results (Figs. 10 and 11) show good agreement between the observed and predicted values below λ/T_r of 12. However, above this frequency significant deviations occur. For cylindrical chambers, it should be noted that

$$\bar{M}\lambda/T_r = \pi f/f_a \tag{11}$$

The tests in the auxiliary chamber were conducted with higher Mach number flows (i.e., 0.03 vs 0.01) than the tests in the combustion chamber. Thus, while the deviations occurred at lower λ/T_r values, they occurred at approximately the same values

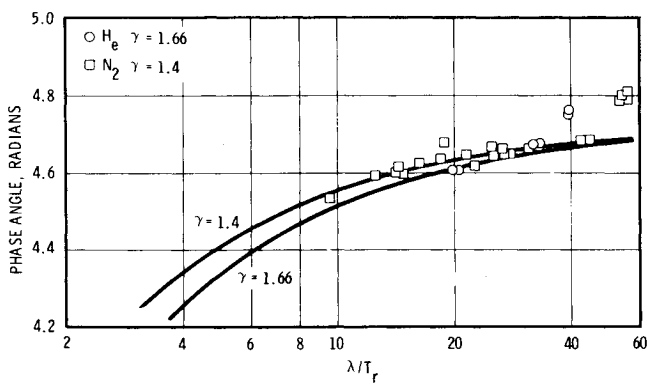

Fig. 9 Cold flow phase response of the combustion chamber.

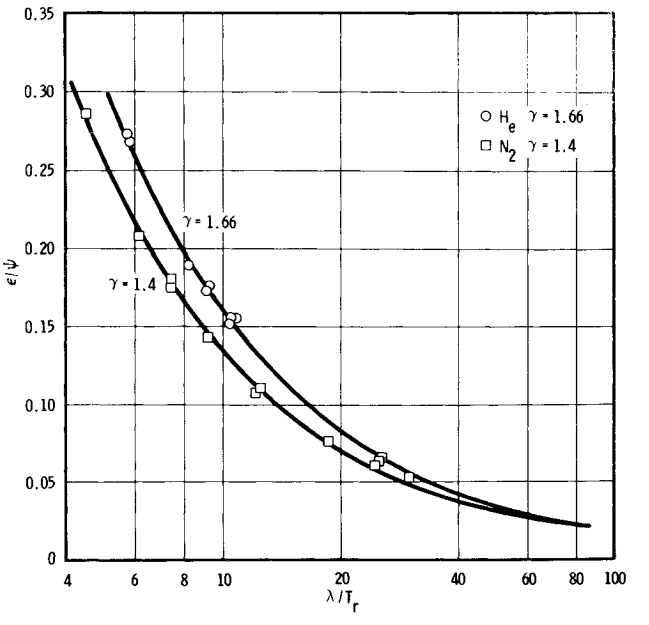

Fig. 10 Cold flow amplitude response of the auxiliary chamber.

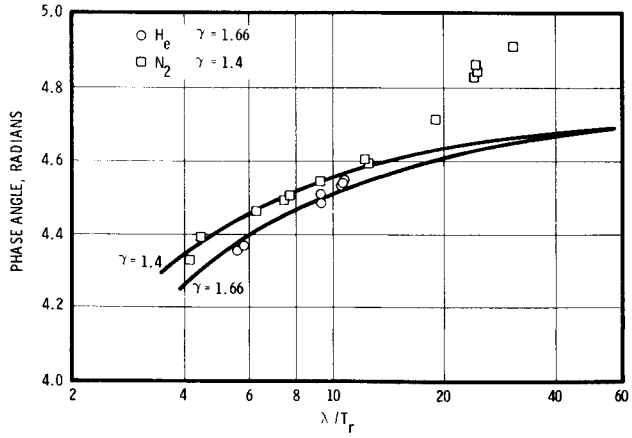

Fig. 11 Cold flow phase response of the auxiliary chamber.

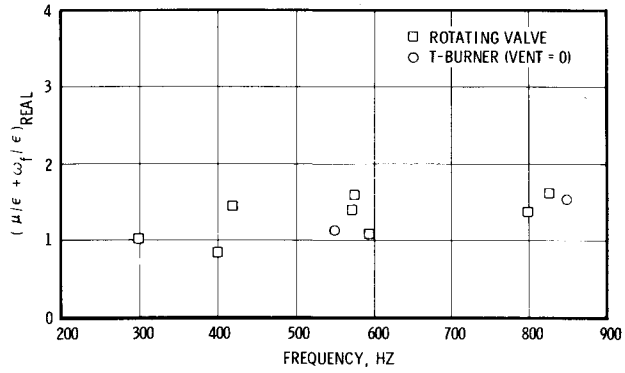

Fig. 13 Combustion response of UTP-3001 at 340 psia.

of f/f_a. Therefore, these results are consistent with an upper frequency limit of $f/f_a = 0.25$. For nitrogen, this frequency limit is 400 Hz, while for helium, the limit is 900 Hz in the auxiliary chamber.

These results confirm the oscillating pressure in this auxiliary chamber can be used as a basis for measuring the phase angle between the combustion chamber pressure and the port area, provided $f/f_a < 0.25$. To eliminate momentum effects, it was necessary to use helium in the auxiliary chamber when combustion tests were conducted at frequencies above 350–400 Hz. At lower frequencies, nitrogen was used.

Propellant Tests

Having established the validity of the chamber ballistics model, a series of tests was conducted using both aluminized and nonaluminized propellant formulations. The primary purpose was to determine the operating characteristics of the apparatus and to provide data for comparison with T-burner data. The two aluminized propellants selected for testing were: ANB 3066, the propellant used in the recent Air Force-sponsored T-burner round robin,[5-10] and UTP-3001, a UTC propellant formulation for which UTC obtained T-burner data using the combined pulse variable-area method. In addition, three nonaluminized propellant formulations were tested: A-13, a 76% loaded PBAN propellant which was used in the JANNAF T-burner round robin test program[21] and was tested extensively at NWC[22]; UTX-8501, a 78% CTPB propellant, which was tested in the T-burner at UTC under Contract DA-04-200-AMC 968(X)[23]; and A-87, the standard JANNAF nonaluminized formulation.

The first series of tests was designed to evaluate the rotating valve hardware and the phase angle measuring system. This effort included evaluation of the electrostatic area sensor probe, the seals separating the probe from the combustion gases, and the design of graphite rotor sleeves and inserts. The major difficulty was found to be the sealing of the electrostatic area sensor from the combustion gases. This problem was never completely eliminated, although substantial improvements were made by moving the sealing O-ring as far as possible from the exhaust ports. Frequent changes of the sealing O-ring also were required.

It also was expected that problems would result from alumina buildup in the graphite inserts and rotor sleeves. However, the problem was not as severe as expected. The graphite rotor sleeves could be used for several tests before erosion of the graphite between the rotor ports became excessive. It was necessary to clear the slot in the graphite insert after each test; however, the buildup was never excessive during a test and erosion of the slot was never a problem.

After the development of the apparatus was successfully completed, a second series of tests was conducted for providing data to compare with T-burner results. Figures 12–16 show the results of these comparison tests, along with comparable T-burner data. To make these comparisons, the T-burner data were reduced assuming the vent term to be zero, i.e., the response function was derived using the expression

$$\alpha_g = 4f(\gamma \bar{M}_b)[Re(\mu/\varepsilon + \omega_f/\varepsilon) - (\gamma - 1)/\gamma] + \alpha_d \qquad (12)$$

The temperature correction proposed in the JANNAF T-burner Manual[21] also was incorporated in the data reduction process.

For the ANB 3066 tests, propellant grains were manufactured from 0.5-gal ice cream cartons taken from the same master-batch used in the Air Force round robin.[5-10] Similarly, the T-burner and rotating valve grains of UTP-3001 were both taken from the same batch of propellant. The A-13 was manufactured at UTC using the mix procedure in the JANNAF T-burner Manual. T-burner tests were conducted with UTC-produced A-13 and the results consistently duplicated the data reported in the JANNAF T-burner Manual. (The A-13 T-burner data shown in Fig. 14 are UTC's contribution to the JANNAF round robin tests.) Thus, batch-to-batch variations are essentially eliminated for these three propellant formulations. The data are tabulated in Ref. 24.

In the T-burner, there is both theoretical[12] and experimental[24] evidence that the combustion response depends on the orientation of the grain relative to the acoustic velocity. This appears to be particularly true for aluminized propellants.[5-10,24] The comparisons shown in Figs. 12 and 13 for the aluminized ANB 3066 and UTP-3001 are based on sidewall T-burner tests. For A-13, Price has shown that grain orientation has no effect on the combustion response.[24] Hence, the endwall T-burner data can be used in comparison shown in Fig. 14.

It should be noted that the majority of these tests were conducted at frequencies above 300 Hz, particularly with the

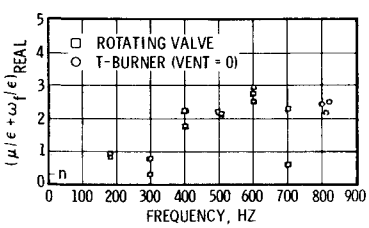

Fig. 12 Combustion response of ANB 3066 at 490–530 psi.

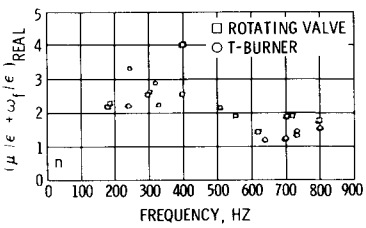

Fig. 14 Combustion response of A-13 at 200–230 psi.

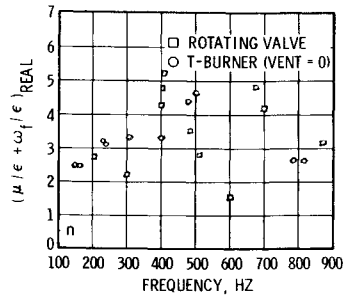

Fig. 15 Combustion response of UTX-8501 at 200 psi.

aluminized formulations. Below 300 Hz, the pressure amplitudes were greater than 10% of the mean chamber pressure. There is some evidence[4] which indicates that nonlinear combustion effects can become significant at these higher amplitudes. Thus, the lower frequency limit was considered to be 300 Hz for the configuration used in these studies.

Reviewing Figs. 12–16 the T-burner and rotating valve yield identical results for ANB 3066, UTP-3001, and A-13. For UTX-8501 and A-87, the results are not as consistent. The UTX-8501 data obtained in the rotating valve show considerable scatter, although the general trend appears to agree with earlier T-burner results. It was noted that ANB 3066, UTP-3001, A-13, and UTX-8501 had the expected burning rates. However, the c^* obtained with UTX-8501 was approximately 50% of the theoretical value, while measured c^* for A-13, UTP-3001, and ANB 3066 were typically 90%–95% of the theoretical value. Furthermore, considerable difficulty was encountered with porosity in the UTX-8501 grains. In view of these difficulties, the scatter shown in Fig. 15 is believed to be the result of variable propellant combustion and physical properties and not a difficulty with the rotating valve.

The A-87 results shown in Fig. 16 also are open to some question. The burning rates measured in the rotating valve were 25% higher than those reported by NWC with their T-burner data. The A-87 used in the rotating valve tests was manufactured at UTC using the JANNAF mix procedure. Hence, the two propellant batches were not ballistically similar and batch-to-batch differences appear to be significant. If the two curves were plotted as $f/\dot{r}_0^2$ as suggested by the thermal wave theory, then the maximum response value would occur at the same frequency parameter. However, the magnitude of the maximum still differs. Noting the extremely low combustion pressure and the burning rate differences, the differences shown in Fig. 16 appear to be batch differences and not necessarily related to the different testing method.

Conclusions and Recommendations

Taking the data shown in Figs. 12–16, the results show the rotating valve is a valid method for measuring the combustion response of solid propellants. Eliminating the propellants which show batch-to-batch differences, there is excellent agreement between the two methods. When different batches of propellant were used in the two test methods, differences between the results were noted. Thus, it appears that for the two non-aluminized propellants, batch-to-batch differences may be significant.

From the results available to date, a comparison of the rotating valve concept with the T-burner suggests the rotating valve approach offers a number of improvements over the T-burner. First, the number of tests required and the labor necessary to conduct the test to obtain a response function value is reduced. Two or three tests at each pressure and frequency condition are sufficient to obtain response function data from the rotating valve. On the other hand, the T-burner method requires 15–20 tests at each pressure and frequency condition.[11]

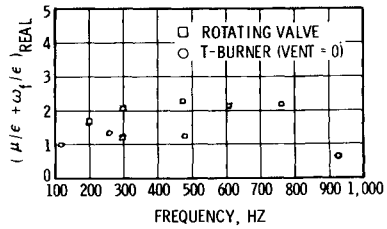

Fig. 16 Combustion response of A-87 at 55 psia.

A second advantage is that propellants can be evaluated for dynamic behavior at the same time that burning rate behavior is being determined. The valve attaches directly to micromotors which are used to evaluate ballistic performance. Thus, for minor increases in cost and time, the combustion dynamics can be determined along with the steady-state measurements. This is particularly important in propellant development programs and in cases where nonuniform propellant ballistics occur (i.e., high solids loaded propellants).

A third improvement offered by the rotating valve concerns the ballistic conditions of the testing. Testing is conducted under rocket motor conditions which minimizes the energy loss to hardware components. T-burner testing, particularly at low frequency, involves hardware with large surface areas which are exposed to the hot combustion gases. The data obtained with nonmetallized propellants have shown significant energy loss effects at frequencies below 800 Hz. These losses are sufficient to change the frequencies and thereby complicate the data analysis. In the rotating valve, these effects are minimized by eliminating the large areas of metal surface exposed to the combustion gases.

In view of the encouraging results, the rotating valve method can be considered as an alternative method to the T-burner for evaluating the dynamic combustion properties of solid propellants. The advantages of reduced cost permit evaluation of several candidate formulations within reasonable cost limits. Thus, combustion stability characteristics now can be considered as one of the evaluation criteria in the final propellant selection process.

The results obtained on this program also have demonstrated the potential for extending response function measurements to lower frequencies. With the current configuration, excessive oscillating pressure amplitudes were measured below 300 Hz. However, by simple apparatus modifications, this lower frequency limit can be extended down to 50–100 Hz with little difficulty.

Appendix: Detailed Theoretical Development

Consider a small rocket motor with a rotating exhaust valve operation in conjunction with a conventional nozzle. Because the motor is small compared to the acoustic wavelength, pressure disturbances are distributed very rapidly throughout the chamber, and the pressure is spatially uniform. Under these conditions, the mass balance for the chamber is [1-3]

$$\frac{d(\rho V_c)}{dt} = \rho_p \dot{r} A_b - g_c P A_t / c^* \tag{A1}$$

The corresponding energy balance is

$$\frac{d(C_v \rho V_c T)}{dt} = \rho_p \dot{r} A_b C_p T_f - g_c P A_t C_p T / c^* \tag{A2}$$

Normalizing these equations to the steady-state mass and energy flow conditions (indicated by the subscript 0) yields

$$\left(\frac{V_c c_0^*}{g_c R T_0 A_{t0}}\right)\left(\frac{T_0}{T}\right)\left\{\frac{d(P/P_0)}{dt} - \frac{(P/P_0)}{(T/T_0)}\frac{d(T/T_0)}{dt}\right\} = \frac{\dot{r}}{\dot{r}_0} - \left(\frac{P A_t c_0^*}{P_0 A_{t0} c^*}\right) \tag{A3}$$

$$\left(\frac{C_v}{C_p}\right)\left(\frac{V_c c_0^*}{g_c R T_0 A_{t0}}\right)\frac{d(P/P_0)}{dt} = \left(\frac{\dot{r}}{\dot{r}_0}\right)\left(\frac{T_t}{T_{t0}}\right) - \left(\frac{P A_t c_0^* T}{P_0 A_{t0} c^* T_0}\right) \tag{A4}$$

For small amplitude oscillations assume

$$\dot{r}/\dot{r}_0 = 1+\mu' = 1+(\mu/\varepsilon)\varepsilon' \quad \text{(A5a)}$$

$$P/P_0 = 1+\varepsilon' \quad \text{(A5b)}$$

$$T/T_0 = 1+\omega' \quad \text{(A5c)}$$

$$A_t/A_{t_0} = 1+\psi' \quad \text{(A5d)}$$

$$c^*/c_0^* = (T/T_0)^{1/2} = (1+\omega')^{1/2} \cong 1+\omega'/2 \quad \text{(A5e)}$$

$$T_f/T_{f_0} = (1+\omega_f') \quad \text{(A5f)}$$

Substituting and letting

$$\gamma = [C_v/C_p]^{-1}$$

$$T_r = 4\alpha g_c A_{t_0} RT_0/V_c c_0^* \dot{r}_0^2$$

$$\tau = t\dot{r}_0^2/4\alpha$$

Equation (A3) becomes

$$\frac{1}{T_r(1+\omega')}\left\{\frac{d\varepsilon'}{d\tau} - \frac{(1+\varepsilon')}{(1+\omega')}\frac{d\omega'}{d\tau}\right\} = 1+\left(\frac{\mu}{\varepsilon}\right)\varepsilon' - \frac{(1+\varepsilon')(1+\psi')}{(1+\omega'/2)} \quad \text{(A6)}$$

Equation (A4) becomes

$$\frac{1}{\gamma T_r}\frac{d\varepsilon'}{d\tau} = \left[1+\left(\frac{\mu}{\varepsilon}\right)\varepsilon'\right](1+\omega_f) - \frac{(1+\varepsilon')(1+\psi')(1+\omega')}{(1+\omega'/2)} \quad \text{(A7)}$$

While Eq. (A3) becomes

$$\frac{1}{T_r}\left\{\frac{d\varepsilon'}{d\tau} - \frac{(1+\varepsilon')}{(1+\omega')}\frac{d\omega'}{d\tau}\right\} = \left[1+\left(\frac{\mu}{\varepsilon}\right)\varepsilon'\right](1+\omega') - \frac{(1+\varepsilon')(1+\omega')(1+\psi')}{(1+\omega'/2)} \quad \text{(A8)}$$

Combining Eqs. (A7) and (A8)

$$\frac{1}{T_r}\left\{\frac{d\varepsilon'}{d\tau} - \frac{(1+\varepsilon')}{(1+\omega')}\frac{d\omega}{d\tau}\right\} = \frac{1}{\gamma T_r}\frac{d\varepsilon'}{d\tau} + (\omega'-\omega_f')\left[1+\left(\frac{\mu}{\varepsilon}\right)\varepsilon'\right]$$

$$\frac{1}{T_r}\left\{\left(\frac{\gamma-1}{\gamma}\right)\frac{d\varepsilon'}{d\gamma} - \frac{1+\varepsilon'}{1+\omega'}\frac{d\omega'}{d\tau}\right\} = (\omega'-\omega_f)\left[1+\left(\frac{\mu}{\varepsilon}\right)\varepsilon\right] \quad \text{(A9)}$$

From Eq. (A7) by expanding and neglecting cross product terms

$$\frac{1}{\gamma T_r}\frac{d\varepsilon'}{d\gamma} = 1+\left(\frac{\mu}{\varepsilon}\right)\varepsilon' + \omega_f - 1 - \varepsilon' - \psi' - \omega' + \tfrac{1}{2}\omega' = \left(\frac{\mu}{\varepsilon}\right)\varepsilon' + \omega_f - \varepsilon' - \psi' - \frac{\omega'}{2} \quad \text{(A10)}$$

Assuming the time dependence of the oscillating quantities to be $\exp(i\gamma\lambda\tau)$, then Eqs. (A9) and (A10) become

$$\left\{1+\frac{i\lambda}{T_r}\right\}\omega = \omega_f + \left(\frac{\gamma-1}{\gamma T_r}\right)i\lambda\varepsilon \quad \text{(A11)}$$

$$\frac{i\lambda\varepsilon}{\gamma T_r} = \left\{\left(\frac{\mu}{\varepsilon}\right)+\frac{\omega_f}{\varepsilon}\right\}\varepsilon - \left\{1+\frac{\psi}{\varepsilon}+\frac{1}{2}\frac{\omega}{\varepsilon}\right\}\varepsilon \quad \text{(A12)}$$

Combining Eqs. (A11) and (A12)

$$\frac{\psi}{\varepsilon} = \left(\frac{\mu}{\varepsilon}\right) - 1 + \frac{\omega_f}{\varepsilon}\left\{\frac{0.5+i\lambda/T_r}{1+i\lambda/T_r}\right\} - \frac{0.5[(\gamma-1)i\lambda/\gamma T_r]}{(1+i\lambda/T_r)} - \frac{i\lambda}{\gamma T_r} \quad \text{(A13)}$$

Note if $\lambda/T_r \gg 1$, then

$$\frac{\psi}{\varepsilon} \approx \left(\frac{\mu}{\varepsilon}\right) - 1 + \frac{\omega_f}{\varepsilon} - 0.5\frac{(\gamma-1)}{\gamma} - \frac{i\lambda}{\gamma T_r} \quad \text{(A14)}$$

References

[1] Denison, M. R. and Baum, E., "A Simplified Model of Unstable Burning in Solid Rocket Propellants," *ARS Journal*, Vol. 3, No. 6, March 1961, pp. 1112–1121.

[2] Friedly, J. C. and Peterson, E. E., "Influence of Combustion Parameters on Instability in Solid Propellant Motors: Part I—Development of Model and Linear Analysis," *AIAA Journal*, Vol. 4, No. 9, Sept. 1966, pp. 1605–1610.

[3] Culick, F. E. C., "A Review of Calculations for Unstable Burning of a Solid Propellant," *AIAA Journal*, Vol. 6, No. 12, Dec. 1968, pp. 2241–2254.

[4] Brown, R. S. and Muzzy, R. J., "Linear and Nonlinear Pressure Coupled Combustion Instability of Solid Propellants," *AIAA Journal*, Vol. 8, No. 8, Aug. 1970, pp. 1492–1500.

[5] Price, E. W., Mathes, H. B., Zurn, D. E., and Brown, B. G., "Combustion Instability of Aluminized Propellants," Rept. NWC TP 5060, April 1971, Naval Weapons Center, China Lake, Calif.

[6] Beckstead, M. W. et al., "Variable Area T-Burner Investigation," Rept. AFRPL-TR-72-85, Dec. 1972, Hercules, Inc., Magna, Utah.

[7] Peterson, J. A. et al., "Pressure Oscillation Investigation for Minuteman III," Rept. AFRPL-TR-72-98, Jan. 1973, Thiokol Chemical Corp., Brigham City, Utah.

[8] Derr, R. L., "Development and Evaluation of Variable Area T-Burner," Rept. AFRPL-TR-72-97, Nov. 1972, Lockheed Propulsion Co., Redlands, Calif.

[9] Micheli, P. L., "Evaluation of Pulsed T-Burner for Metallized Propellants," Rept. AFRPL-TR-72-54, Sept. 1973, Aerojet Solid Propulsion Co., Sacramento, Calif.

[10] Wendelken, C. P., Chew, T. J. C., and Weiss, R. R., "Combustion Instability Characteristics of Several Solid Propellant Rocket Propellants for Booster and Tactical Rocket Applications," presented at the 9th JANNAF Combustion Conference, Monterey, Calif., Sept. 11–15, 1972.

[11] Andrepont, W. C. and Schoner, R. J., "The T-Burner Test Method for Determining the Combustion Response of Solid Propellants," AIAA Paper 72-1053, New Orleans, La., 1972.

[12] Culick, F. E. C., "Interactions Between the Flow Field Combustion and Wave Motions in Rocket Motors," Rept. NWC TP 5349, June 1972, Naval Weapons Center, China Lake, Calif.

[13] Coates, R. L., "Application of Hart-McClure Analysis to Interpretation of T-Burner Data," presented at the 3rd AFRPL Workshop on Combustion Instability, Sacramento, Calif., Oct. 1971.

[14] Beckstead, M. W. and Price, E. W., "Nonacoustic Combustor Instability," *AIAA Journal*, Vol. 5, No. 11, Nov. 1967, pp. 1989–1996.

[15] Beckstead, M. W. and Culick, F. E. C., "A Comparison of Analysis and Experiment for Solid Propellant Combustion Instability," Rept. TP 4531, May 1968, Naval Weapons Center, China Lake, Calif.

[16] Coates, R. L., Cohen, N. S., and Hervill, L. R., "An Interpretation of L^* Combustion Instability in Terms of Acoustic Instability Theory," *AIAA Journal*, Vol. 5, No. 6, June 1967, pp. 1097–1102.

[17] Barrère, M. and Nadaud, L., "Provision of Unstable Operation Domains of Solid Propellant Rocket Motors," Paper 72-1052, presented at 22nd International Congress of Astronautics, Brussels, Sept. 20–25, 1971.

[18] Eisel, J. L., Ryan, N. W., and Baer, A. D., "Spectoral and Temporal Resolution of Propellant Flames During Bulk Mode Instability," presented at 8th JANNAF Combustion Conference, Monterey, Calif.; also CPIA Publication 220, Nov. 1971, Silver Spring, Md.

[19] Cantrell, R. H. and Hart, R. W., "Interaction Between Sound and Flow in Acoustic Cavities: Mass, Momentum, and Energy Considerations," *Journal of Acoustical Society of America*, Vol. 36, No. 4, 1964, pp. 697–706.

[20] Culick, F. E. C. and Dehority, G. L., "An Analysis of Acoustic Waves in a Cold Flow Rocket," NWC TP 4544, May 1968, Naval Weapons Center, China Lake, Calif.

[21] Culick, F. E. C., "T-Burner Manual," CPIA Publication 191, Nov. 1969, Silver Spring, Md.

[22] Price, E. W. et al., "Experimental Studies on Oscillatory Combustion of Solid Propellants," Rept. NWC TP 4393, March 1969, Naval Weapons Center, China Lake, Calif.

[23] Brown, R. S., Muzzy, R. J., and Steinle, M., "Surface Reaction Effects on the Acoustical Response of Composite Solid Propellants," *AIAA Journal*, Vol. 6, No. 3, March 1968, pp. 479–488; also see Final Rept. Contract DA-04-200-AMC-96F(X), Sept. 1968, United Technology Center, Sunnyvale, Calif.

[24] Price, E. W., "NWC Experimental Work Related to Acoustical Mean Flow Interactions (and Other Effects Related to Interaction Measurement)," NWC TN 608-122, March 1973, Naval Weapons Center, China Lake, Calif.